RSC Advances

ROYAL SOCIETY OF CHEMISTRY

www.rsc.org/advances

Journal Name

ARTICLE

A one-pot synthesis of nanostructured mesoporous TiO_2 films on graphite felt substrates for fast catalysis

Received 00th January 20xx,
Accepted 00th January 20xx

DOI: 10.1039/x0xx00000x

www.rsc.org/catalysis

S. El-Kacemi,[a,b] Mar. Es-Souni,[a,c] S. Habouti,[a] D. Schopf,[a] M. Hamdani[b] and M. Es-Souni*[a]

In the present paper we report a one-pot synthesis of nanocrystalline, crack-free and mesoporous thin TiO_2 films on graphite felt (GrF) and GrF terminated with NiO nanoleaflets. The films are obtained using an immersion method in an ethanolic solution of titanium isopropoxide containing small amount of NH_3 catalyser. A short heat treatment at 450 °C yields pure phase anatase directly on GrF or on the NiO nanoleflets. The method allows processing of a variety of TiO_2/metal oxide heterostructures and can be implemented for other catalysts. The supported films were tested for their photocatalytic activity using a continuous-flow set-up of an aqueous amido black solution under a cold UV diode at 360 nm. The results are compared to those of a thick macro-mesoporous P25-TiO_2 film on Si. Full discoloration of the dye is obtained within 50 to 120 minutes for the films on the GrF substrates. The discoloration kinetics show a non-linear behaviour that is interpreted in terms of the rapid rarefication of the dye molecules. In contrast the P25-TiO_2 film on Si shows the usual linear behaviour with a small rate constant. The high discoloration rate is obtained with TiO_2 directly deposited on GrF. Based on latest literature findings, it is postulated that the high defect density of the graphite structure could promote better charge separation and higher photocatalytic activity in comparison to GrF/NiO/TiO_2 heterostructure.

Introduction

The photocatalytic properties of TiO_2 are very well-known, have garnered immense research activities and continue to attract huge interest. The application potentials reach from indoor air purification to waterlysis.[1-3] Water purification is particularly of acute actuality because of dwindling water reserves in many regions of the world and the ensuing necessity to recycle waste waters.

At the origin of the photocatalytic activity of TiO_2 in all its polymorphs is the creation of electron-hole pairs upon irradiation with high energy photons, in general with energy in excess of 3.2 eV, i.e. in the UV range. A draw-back of pure TiO_2 is however the high recombination rate of charge carriers that limits yield of photocatalytic reactions. Strategies have been implemented to limit carrier recombination via TiO_2-noble metal and/or TiO_2-semi-conductor oxide or quantum dot heterojunctions.[4-7] However, one prerequisite for efficient (photo)catalysis is the availability of surface sites. One possibility to fulfil this requirement is the use of nanopowders. But they require filtration that constitutes a serious disadvantage as to cost and poor recycling yield. Porous films may provide a more advantageous alternative, although the required macro-mesoporosity (to achieve high density of active sites) may be difficult to achieve which may result in poor photocatalytic reaction yield.[8,9] The use of high-surface area substrates such as porous activated carbon[10] or graphite fibers[11] is another promising alternative, and indeed few reports outline the high photocatalytic activity and good recyclability of TiO_2 on these substrates.[12] Deposition of TiO_2-films on carbon materials has been achieved via different methods, among them ionized cluster beam (starting from high purity Ti-metal)[11], molecular adsorption deposition (MAD, starting from $TiCl_4$)[12], and other methods based on hydrolysis of titanium isopropoxide (TIIP) or impregnation using TiO_2 powder.[10] The coatings obtained were of various thickness, morphology and coverage, with the MAD technique enabling better coverage, although the films were interspersed with micro-crack (see Fig. 2 in Reference 12).

In the present work we propose a one-pot soft chemistry method for the homogeneous coating of graphite felt (GrF) substrates with thin TiO_2 films starting from a highly diluted ethanolic solution of TIIP that is subsequently subjected to controlled hydrolysis at room temperature. Variants of this method that are also reported here include the deposition of NiO/TiO_2 heterostructures on GrF. The method also allows deposition of noble metal-TiO_2 nanocomposites. The photocatalytic activity of the different heterostructures is tested on amido black dye solution in a continuous flow set-up under a cold UV diode of 360 nm wave length. The choice of this dye has been made based on its widespread use for dying textile fibres, in biochemistry and because of its toxicity and pollution of waters. The results are compared to those obtained on a thick TiO_2 film that was made using a hybrid sol-

[a] Institute for Materials & Surface Technology, University of Applied Sciences, Kiel, Germany. E-Mail: mohammed.es-souni@fh-kiel.de
[b] Electrochemical Lab, Ibn-Zohr University, Agadir, Morocco
[c] Faculty of Dentistry, Christian-Albrecht-University, Kiel, Germany
† Electronic Supplementary Information (ESI) available. See
DOI: 10.1039/x0xx00000x

gel-P25 powder-method.[9] All the films deposited on GrF show superior photocatalytic activity with almost full degradation within 60 minutes.

Experimental

Chemicals

The following chemicals were used as purchased: Titanium(IV)-Isopropoxide (TTIP, 97 %, Aldrich, Germany), Ethanol (99 %, Walter, Germany), Ammonia (25 %, Roth, Germany), Nickel(II)Chloride ($NiCl_2$ $6H_2O$, Aldrich, Germany), Hexa-methylenetetramine (Aldrich, Germany), Polyethylenimine (Aldrich, Germany), Absolute Ethanol (Merck, Germany), Hydrochloric Acid (37 %, Roth, Germany).

Preparation of GrF substrates and films

GrF substrates (Alapha Aisar), 2 mm thick were cut in pieces of 2x2 cm^2; they were first treated in a mixture of sulfuric acid and hydrogen peroxide to remove residual organic products, and subsequently thoroughly rinsed in deionized water and dried. A short treatment at 650 °C for 30 minutes has proven to confer macroporosity and hence high surface area to the GrF fibers. Furthermore, the substrates were highly hydrophilic after this treatment which is a prerequisite for successful coating. Henceforth all GrF substrates were subjected to this treatment before coating.

TiO_2 thin films were either prepared on bare GrF or GrF/$Ni(OH)_2$ -nanolamellae with high surface area. For $Ni(OH)_2$ on GrF substrates a growth solution was first prepared as follows: $NiCl_2$ $6H_2O$ (0.18 g, 40 mM, pH = 3.60) and HMTA (0.14 g, 50 mM, pH = 6.72) were dissolved by stirring (5 min) in 20 ml of water followed by sequential and drop-wise addition of PEI (75 µl, pH = 6.80) and 25 % NH_4OH (6 ml, pH = 12.25), and further stirring for 10 min. In a typical experiment the inclined GrF substrate was placed in a flask, covered with a para film let to react 2 hours at 85-88 °C using an oil bath. Subsequently the nanolamellae anchored on the substrate were thoroughly rinsed with de-ionized water, blown dry in air and kept 18 h in a dry box at 100 °C.

Thin TiO_2 films were prepared on each of the GrF substrates depicted above by immersion in a precursor solution that was prepared as follows: solution A containing 5 ml Ethanol (99 %) and 25 µl ammonium hydroxide solution (25 %) was added dropwise to solution B containing 5 ml Ethanol (99 %) and 295 µl titanium (IV) isopropoxide and stirred for 20 s. The GrF substrates were then immersed in the precursor solution kept at room temperature until the solution starts to be lightly turbid, generally in 20 to 30 min. The substrates were then removed from the solution, cleaned in ethanol, dried and finally heat treated in a pre-heated furnace at 450 °C for 60 min. The coating sequence is repeated 3 times to ensure full coverage. For comparison macro-mesoporous thick TiO_2 films were prepared on silicon substrates using a hybrid powder P25-sol-gel procedure described in our previous paper.[8]

Characterization

The samples were investigated by X-ray diffraction (XRD) (X'Pert Pro, PANalytical, Holland) in grazing incident geometry with fixed angle of 1.5°, and 0.05° step using monochromatic Cu Kα radiation (λ = 1.5418 Å) and a scanning range (2θ) of 10–90°. A Bruker Raman microscope (532 nm laser diode) was used to acquire spectra over a wave number range of 70−3700 cm^{-1}, with a spectral resolution of 3-5 cm^{-1}, using a backscattering configuration with a 20× objective. Data were collected on numerous spots on the sample and recorded with a fully focused laser power of 20 mW or 5 mW in the case of bare Gr. Each spectrum was accumulated ten times with an integration time of 15 s. The Raman signal was recorded using a CCD camera. Silicon substrate Raman peak position (520 cm^{-1}) was used to calibrate spectral frequency. The nano-structured surface was characterized using a high-resolution scanning electron microscope (Ultra Plus, ZEISS, Germany).

Photocatalytic activity

The photocatalytic activity of the different samples was monitored using 1 mM aqueous solutions of amido black (AB, pH = 5). The photocatalytic set-up is depicted in Fig. 1. It is a continuous flow set-up comprising a quartz cuvette, a peristaltic pump, a funnel-like container, a cold UV LED (Opsytec Dr. Gröbel, Ettlingen, Germany) with a wave length of 360±5 nm and power density of 2 W/cm^2 at a distance of 3 cm from the specimen surface, and finally a spectrophotometer (Spectrum 400, Perkin-Elmer). The solution is pumped onto the specimen surface with the UV LED switched-on and circulated to the quartz cuvette inside the spectrophotometer where measurement is conducted at the maximum absorption wave length of the dye as function of time. As reference a quartz cuvette containing deionized water was used. This set-up ensures a continuous monitoring of dye discoloration without altering the volume of the solution while dye molecules are continuously refreshed on the photocatalyst surface.

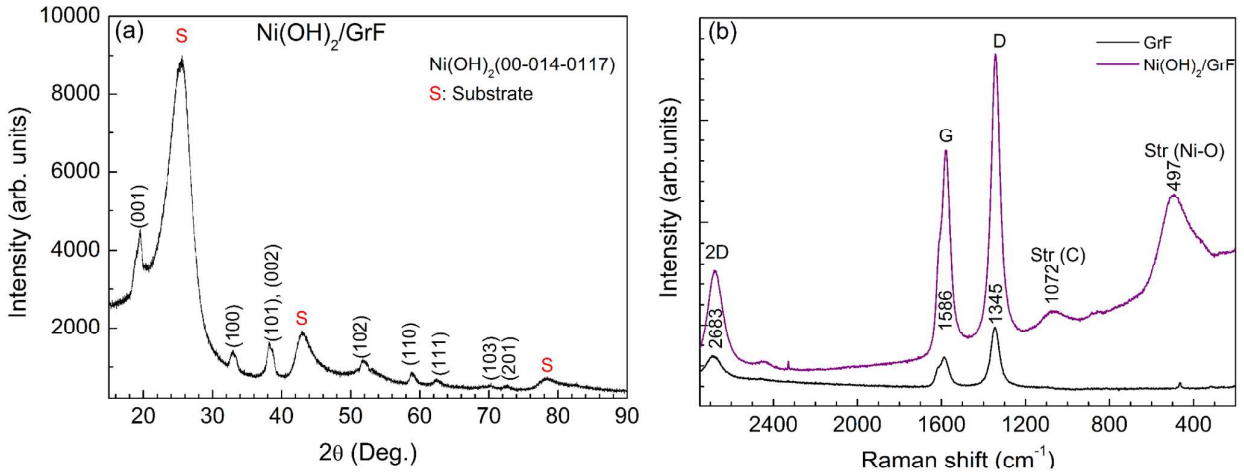

Fig. 2 (a) XRD pattern of $Ni(OH)_2$ on GrF (S); (b) Raman scattering spectra of bare GrF (lower pattern) showing characteristic vibrations of graphite with a high density of defects as suggested by the high D to G band ratio; the upper pattern additionally shows characteristic lines of $Ni(OH)_2$

Results and discussion

Morphology and structure of the substrates

The XRD patterns of the bare graphite felt substrate, pre-treated as outlined in the experimental part above, are displayed in Fig. 2a. They show characteristic peaks of crystalline graphite.[13] The $Ni(OH)_2$ terminated substrate displays characteristic peaks of β-$Ni(OH)_2$ in addition to those of graphite. The diffraction peaks at 19.3°, 33.2°, 38.6°, 59.1°, 62.7°, 70.5°, 72.8°, and 82.6° are attributed to the reflections (001), (100), (101), (110), (111), (103), (201) and (202), respectively, of the β-$Ni(OH)_2$ phase with the hexagonal brucite[14] structure, according to the PDF 00-014-0117.

The Raman scattering spectra of the GrF substrate in the as-received state, Fig. 2b, show characteristic lines at 1342 cm^{-1}, 1573 cm^{-1} and 2667.5cm^{-1} that are attributed to the defect-characteristic D band , the sp^2-network band E_{2g} (G) and overtone D* of the D band, respectively.[14] When GrF is treated as outlined above the intensity of the D band increases, and the intensity ratio I_D/I_{D*} increases with maximum for the heat treated state denoting increasing defects and nanocrystallite formation.[15] The I_D/I_G intensity ratio has been shown to

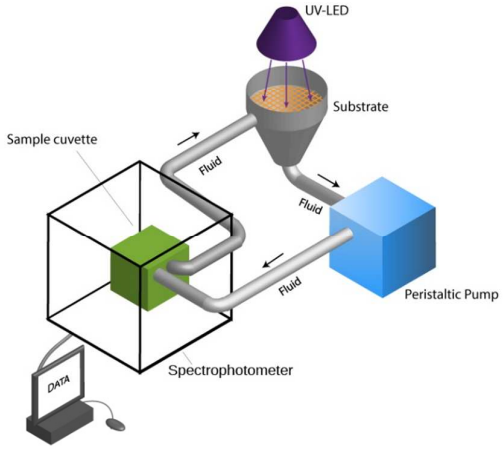

Fig. 1 A schematic drawing of the continuous-flow experimental set-up for monitoring the photocatalytic activity.

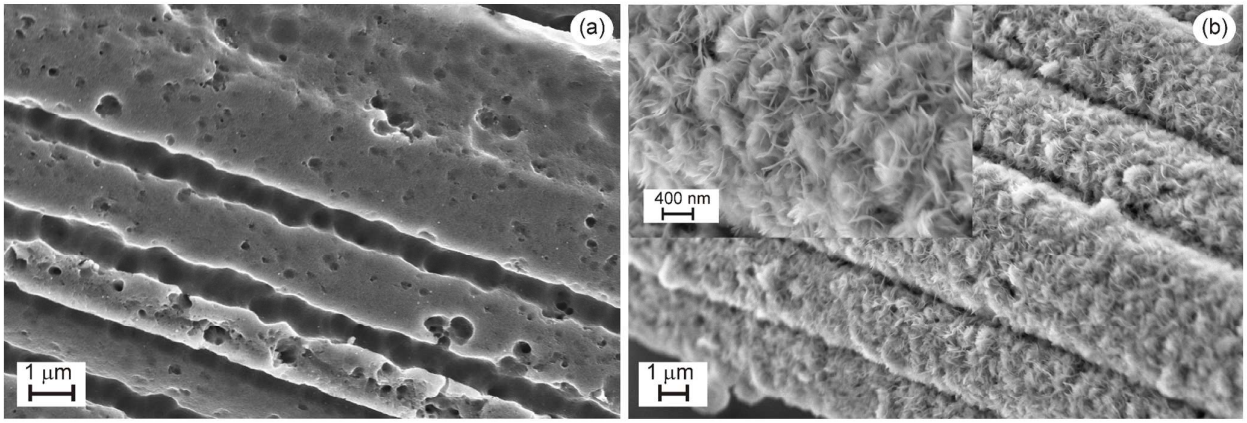

Fig. 3 SEM micrographs of the different substrate microstructures. (a) GrF heat treated at 650 °C showing porosity; (b) GrF terminated with one layer of $Ni(OH)_2$ nanolamellea. The inset shows the leaflet structure.

correlate with crystallite size through the empirical formula[15]

$$La(nm) = (2.4\times10^{-10})\lambda^4\left(\frac{I_D}{I_G}\right)^{-1} \quad (1),$$

where λ is the wave length (in nm) of the laser source (532 nm in our case). The I_D/I_G ratios of the GrF substrates used lead to crystallite size values in the range from 20 to 30 nm. The $Ni(OH)_2$-covered substrates displays Raman lines characteristic of β-$Ni(OH)_2$[14], in agreement with the XRD data. We will not further discuss the Raman lines of $Ni(OH)_2$ as this phase transforms to NiO after deposition of TiO_2 and subsequent annealing (see below).

The different morphologies of the substrates are illustrated in Fig. 3. The short treatment of GrF at 650 °C yields a highly rough surface, Fig. 3a, that is the consequence of selective "burning" of graphite. But this has also the benefit of increasing the surface area of the substrate. The $Ni(OH)_2$ phase forms thin lamellae over the whole graphite fibre surface as depicted in the inset of Fig. 3b, affording a high surface area support for the TiO_2 layer.

Morphology and structure of the TiO_2 films

Fig. 4a exemplary shows the morphology of TiO_2 directly deposited onto GrF after annealing at 450 °C. The films are nanostructured with a mean grain size in the range of 20 to 30 nm, mesoporous and appear to well adhere to the substrate, filling even the interior of the GrF-pores (see Fig. 4c). The films deposited on $Ni(OH)_2$ and subsequently annealed espouse the undelaying leaflet-morphology, as illustrated in Fig. 4d, thus affording more surface area than the previously discussed films.

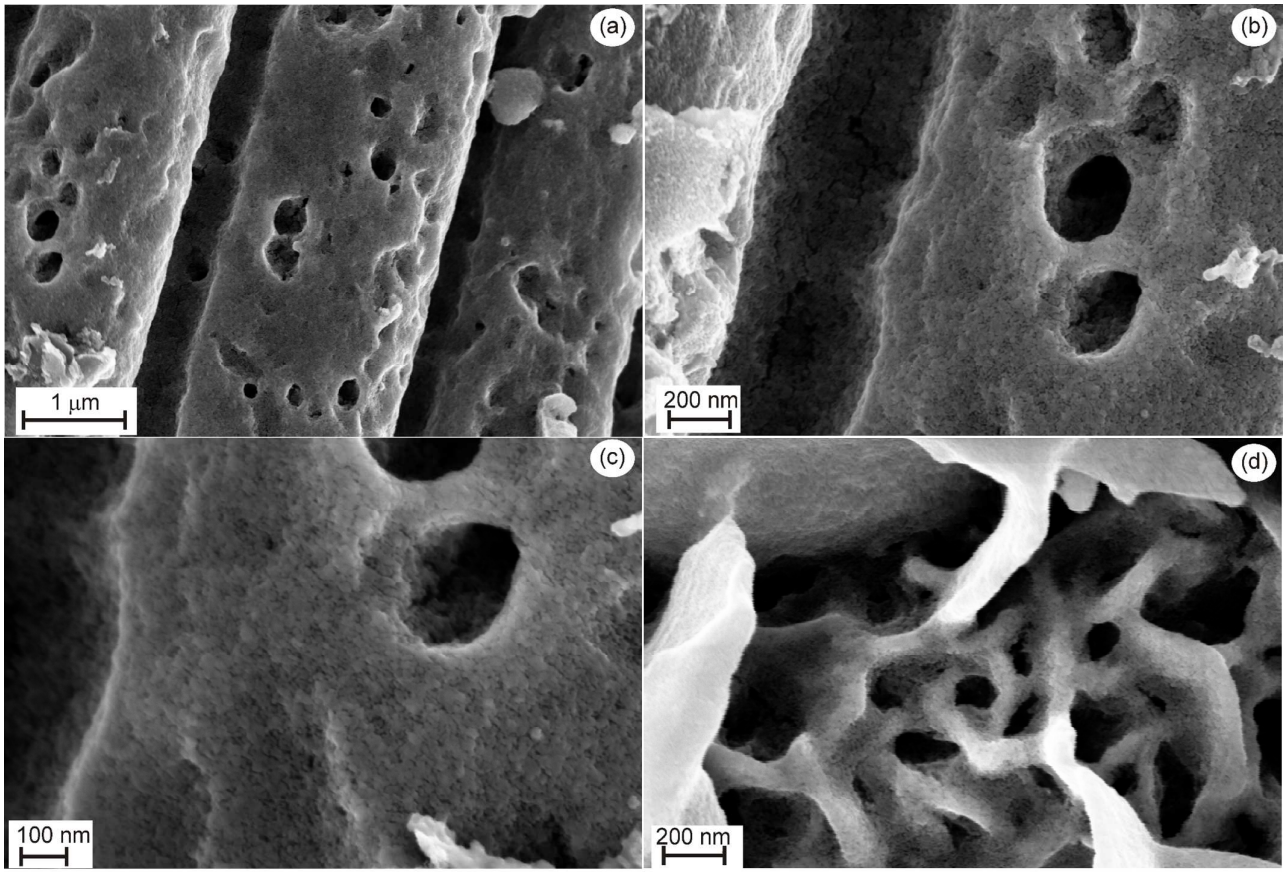

Fig. 4 SEM micrographs of the TiO_2 film morphology on bare GrF (a-c) and $Ni(OH)_2$-terminated GrF. Notice the mesoporous nature of the TiO_2 film that is well visible in (c). Notice also that TiO_2 penetrates the pores.

X-ray diffraction analysis using long acquisition time was necessary in order to detect the weak and broad peaks of TiO_2 shown in Fig. 5a, but the peaks can unambiguously be attributed to anatase despite overlapping of the 100 % 101 peak with the 001 peak of GrF. An even more difficult analysis of the XRD patterns arises when TiO_2 is deposited on $Ni(OH)_2$ (that transforms to NiO upon annealing) because some peak overlapping between NiO and anatase also occurs, Fig. 5b. Unfortunately the broad peaks obtained for anatase do not allow further exploitation, e.g. calculation of the crystallite size using the Scherrer-formula. Raman scattering delivers, in addition to the GrF peaks depicted above, intense peaks that are unambiguously attributed to the anatase phase (the NiO underlayer is not Raman active).

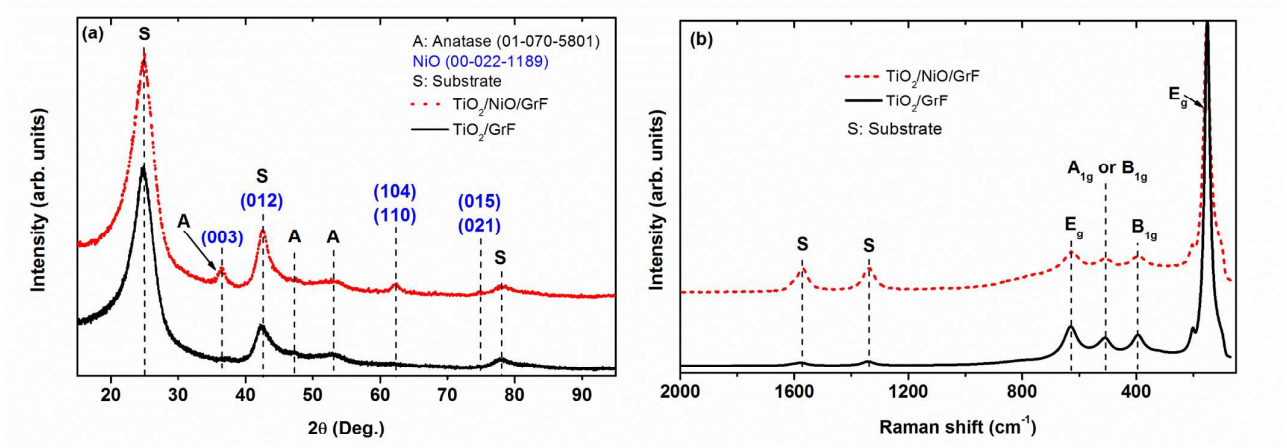

Fig. 5 (a) XRD pattern of TiO_2 on NiO-terminated GrF ($Ni(OH)_2$ transforms to NiO upon heat treatment); (b) Raman scattering of TiO_2 on GrF and on NiO-terminated GrF. The spectra show characteristic vibrations of the anatase phase in addition to the lines of the GrF substrate.

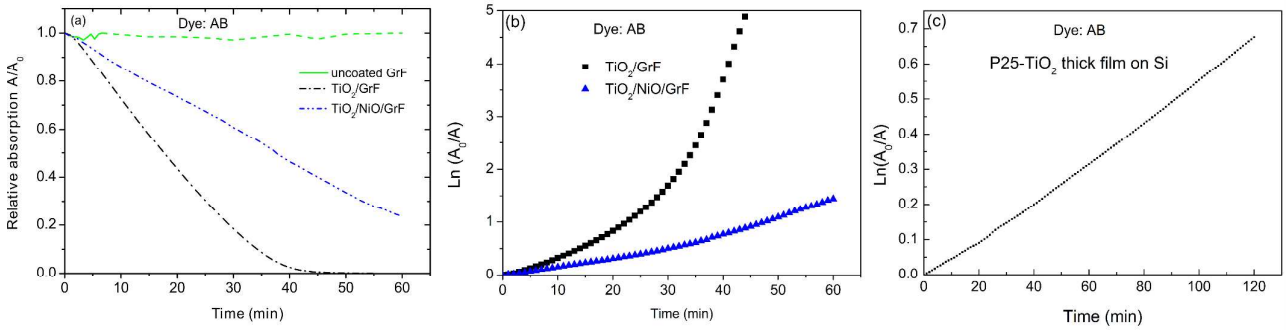

Fig. 6 Photocatalysis experiments using amido black (AB). (a) Relative optical absorption (at the absorption maximum of AB at 620 nm) as function of time; A_0 is the absorption at t=0; the behaviour of the bare GrF substrate under the same conditions is also shown; (b) plot of $Ln(A_0/A)$ as function of time showing approximately two linear segments; (c) plot of $Ln(A_0/A)$ of a thick macro-mesoporous P25-TiO_2-film.

From these results we may state that TiO_2 can be readily deposited as well directly on GrF as on GrF covered with other oxide materials thus allowing heterostructures to be tested. The formation of homogeneous TiO_2 coating on the GrF fibres is catalysed by NH_3 in the ethanolic solution. It is stipulated that NH_3 promotes condensation of negatively charged $(RO)_3TiO^-$ species via a reaction sequence similar that described in References.[16,17] If we suppose that the GrF surface contains hydroxyl-groups after heat treatment that would explain their hydrophilic character (see also below), then we would expect the negatively charged TiO^- species to graft on the surface with the elimination of an alcohol. Similar mechanisms are expected for deposition of TiO_2 on $Ni(OH)_2$. We may also state that substantial diffusion does not take place for NiO-TiO_2 compounds to be formed upon heat treatment[18], but a limited diffusion at the interface is not to be ruled out, resulting in cross-doping of the oxides.

Photocatalytic properties

The degradation of azo dyes on photocatalyst's surface, particularly on TiO_2, has been widely discussed in literature (e.g. see the review article by Konstantinou and Albanis, Reference 3). Highly oxidizing hydroxyl radicals and reducing oxygen radicals react with the cationic dye to full mineralisation (CO_2, SO_4^{2-}, NH_4^+, NO_3^-) via the formation of intermediate products. Discoloration is the consequence of the cleavage of the azo bond (N=N).

The photocatalytic properties of the different heterostructures are displayed in Fig. 6. Overall the kinetic of degradation is rather rapid with full degradation of the dye molecules within 50 to 120 minutes, depending on film heterostructure. These high degradation rates surpass by far the degradation rates obtained on macro-mesoporous TiO_2-P25-thick coatings on silicon reported in our previous work[9] and repeated under the present conditions in Fig. 6c. Although comparison with other work is difficult because of different loadings and experimental photocatalytic conditions the present nanocomposites also override the performances reported for TiO_2 films on activated graphite fibres reported by Fu et al. and Yamashita et al.[11, 12]

But specificities of the different coatings are clearly seen, i.e. the degradation (discoloration) of the dye proceeds with different kinetics: AB is readily degraded on TiO_2/GrF while substantially slower degradation kinetic is observed on TiO_2/NiO/GrF. The specific structure of the support therefore plays a decisive role on the degradation kinetics, and will be discussed below.

The degradation kinetics are generally described by the Langmuir–Hinshelwood (L–H) kinetics model

$$-\frac{dC}{dt} = \frac{kKC}{1+KC} \quad (2),$$

where C (mol/l) is the concentration of the dye, t the irradiation time, k the reaction rate constant and K the adsorption coefficient of the dye. For low dye concentrations in the mM range, which is the case here, Equation 2 may be approximated by:

$$-\frac{dC}{dt} = kKC = k_{eff}C \quad (3)$$

with k_{eff} an effective rate constant. Equation 3 describes a first order reaction that integrates to:

$$Log\frac{C_0}{C} = k_{eff}t \quad (4)$$

Plots of Log (C_0/C) *vs.* time yields for none of the heterostructures on GrF the straight line expected for Equation 4 while straight lines are obtained for the thick TiO_2-P25-coatings on silicon (compare Figs. 6a-b to Fig. 6c). This rather suggests that photodegradation of both dyes using TiO_2-heterostructures on GrF does not follow simple reaction kinetics. However, putting things simply, and regardless of TiO_2/GrF-heterostructure, we may suppose two different photodegradation kinetics, with a fast one, roughly in the first 30 minutes, and a slower one towards the end of reaction. The degradation rates obtained from the two linear segments of the rate curves are summarized in Table 1.

This suggests that the progressive and fast rarefication of the dye on the GrF/TiO_2 heterostructures leads to slower photodegradation rates towards the end of the photocatalytic reaction. Because the reaction kinetics (mineralisation of the dye) depends on the adsorption of the dye molecules on the catalyst surface less molecules are available for the surface coverage at longer times thus leading to a tail in the degradation kinetics (see Fig. 6a). Indeed it has been reported that the degradation rate is very much dependent on the initial concentration of the dye within a certain concentration interval, and was rationalized in terms of the necessity of immediate availability of the dye molecules to react with the short-living oxidizing radicals generated on the oxide surface by UV irradiation.[1-3] Following this reasoning a higher degradation rate is expected for higher initial dye concentration. The case of the thick TiO_2 film that shows linear kinetics throughout the experiment may be understood if we consider that the degradation rate is so slow that the number of adsorbed molecules remains almost constant during the experiment.

The question now arises as to the substantial differences found in the degradation rates associated with the two different heterostructures. As mentioned above some cross-doping is expected for the NiO-TiO_2 nanostructure, although its extent remains unclear. More importantly, however, the build-up of a p-NiO-n-TiO_2 junction should lead to efficient charge separation as NiO is known as hole scavenger.[19]The photocatalytic performance of the GrF/NiO/TiO_2 nanocomposite structure, although superior to that of the thick TiO_2 film, is, nevertheless, inferior to that of GrF/TiO_2. We may speculate that charge separation is more efficient in the GrF/TiO_2 heterostructure that in the NiO-TiO_2 heterojunction. Recent work on graphene/graphene oxide (GO) as catalyst supports suggest that a substantial mole fraction of photo-generated electrons from TiO_2 nanoparticles are transferred to GO.[20] A fraction of these electrons serves to reduce GO to reduced graphene oxide (RGO) with the remainder being stored in the GO or serves to reduce cations, e.g. of noble metals.[20] It is thought that a similar mechanism may hold in the present situation. As outlined above the thermal treatment of the GrF substrates in air induces defects at the surface of the graphite fibres, as attested by the increase in the intensity of the defect D band, which may lead to the formation of GO.[15,21] Upon irradiation with UV light efficient carrier separation occurs because the photo-generated electron are scavenged by GO and can be transferred to oxygen to form highly reactive radicals that explain the higher photocatalytic activity observed for the GrF/TiO_2 samples.

Table 1 Rate constants associated with the different microstructures and kinetics

Film heterostructure	Rate constant (min^{-1}), rapid	Rate constant (min^{-1}), slow
GrF/TiO_2	0.275	0.053
GrF/NiO/TiO_2	0.033	0.016
P25-TiO_2/Si	0.0057 (linear behaviour throughout reaction time)	-

Conclusions

In conclusion we have shown that graphite substrates with high surface area, in particular graphite felt, can be used as supports for catalysts in general and photocatalysts in particular. A one pot synthesis route has been applied using an immersion technique to process nanocrystalline, mesoporous TiO_2 anatase films either directly on GrF or on GrF terminated with $Ni(OH)_2$ nano- leaflet structure. The TiO_2 films are shown to espouse the morphology of the support thus affording a high surface area. The photocatalytic properties obtained with these composite materials are most promising with full degradation/ discoloration of a model dye achieved within less than 60 minutes in the case of TiO_2 directly deposited on GrF. At this stage it seems that achieving heterojunction with other semi-conductor oxides does not necessarily positively impact the properties. Rather a direct contact between, a presumably oxidized, graphite surface and TiO_2 seems to be more effective in terms of carrier separation and photocatalytic activity. The one-pot synthesis devised in this work may be applied to other catalysts and nanocomposites, and should show a way for using cost-effective and active supports together with sustainable bottom-up processing routes for making advanced catalysts.

Acknowledgements

Financial support of this work is provided by the German Federal Ministry of Education and Research (BMBF) for a cooperative project between the University of Applied Sciences Kiel and the University Ibn Zohr in Agadir, Morocco. Project#*MAR10/003; project code 01DH12027*.

References

1 O. Carp, C.L. Huisman and A. Reller, *Progress in Solid State Chemistry*, 2004, **32**, 33.
2 A. Fujishima, T. N. Rao and D. A. Tryk, *Journal of Photochemistry and Photobiology C: Photochemistry Reviews*, 2000, **1**, 1.
3 I.K. Konstantinou, T.A. Albanis, *Applied Catalysis B: Environmental*, 2004, **49**, 1.
4 P. V. Kamat, *J. Phys. Chem. C*, 2007, **111**, 2834.
5 W. Y. Teoh, J. A. Scott and R. Amal, *J. Phys. Chem. Lett.*, 2012, **3**, 629.

6 D.L. Liao, C.A. Badour and B.Q. Liao, *Journal of Photochemistry and Photobiology A: Chemistry*, 2008, **194**, 11.
7 A. Tanaka, S. Sakaguchi, K. Hashimoto and H. Kominami, *ACS Catal.*, 2013, **3**, 79.
8 D. G. Shchukin, and R. A. Caruso, *Chem. Mater.*, 2004, **16**, 2287.
9 J. Mani, H. Sakeek, S. Habouti, M. Dietze and M. Es-Souni, *Catal. Sci. Technol.*, 2012, **2**, 379.
10 A. H. El-Sheikh, A. P. Newman, H. Al-Daffaee, S. Phull,, N. Cresswell and S. York, *Surface & Coatings Technology*, 2004, **187**, 284.
11 H. Yamashita, M. Harada, A. Tanii, M. Honda, M. Takeuchi, Y. Ichihashi, M. Anpo, N. Iwamoto, N. Itoh and T. Hirao, *Catalysis Today*, 2000, **63**, 63.
12 P. Fu, Y. Luan and X. Dai, *Journal of Molecular Catalysis A: Chemical*, 2004, **221**, 81.
13 Z.Q. Li, C.J. Lu, Z.P. Xia, Y. Zhou and Z. Luo, *Carbon*, 2007, **45**, 1686.
14 D. S. Hall, D. J. Lockwood, S. Poirier, C. Bock, and B. R. MacDougall, *J. Phys. Chem. A*, 2012, **116**, 6771.
15 M. A. Pimenta, G. Dresselhaus, M. S. Dresselhaus, L. G. Cançado, A. Jorio and R. Saito, *Phys. Chem. Chem. Phys.*, 2007, **9**, 1276.
16 P. Wang, D. Chen, F-Q. Tang, *Langmuir*, 2006, **22**, 4832.
17 C. J. Brinker and G. W. Scherer, *Academic Press*, 1990, 47-49.
18 W. Laqua, E. W. Schulz and B. Reuter, *Z. Anorg. Allg. Chem.*, 1977, **433**, 167.
19 Z. Wu, Y. Wang, L. Sun, Y. Mao, M. Wang, C. Lin, *J. Mater Chem. A*, 2014, **2**, 8223-8229.
20 Ian V. Lightcap, Thomas H. Kosel, and Prashant V. Kamat, *Nano Lett.,* 2010, **10**, 577.
21 W. Gao, L. B. Alemany, L. Ci and P. M. Ajayan, *Nature Chem.*, 2009, **1**, 403.